



## OPEN

## On chip shapeable optical tweezers

C. Renaut<sup>1,2,3</sup>, B. Cluzel<sup>1</sup>, J. Dellinger<sup>1</sup>, L. Lalouat<sup>1</sup>, E. Picard<sup>2</sup>, D. Peyrade<sup>3</sup>, E. Hadji<sup>2</sup> & F. de Fornel<sup>1</sup>

## SUBJECT AREAS:

OPTICAL MANIPULATION  
AND TWEEZERS

INTEGRATED OPTICS

OPTOFLUIDICS

NANOPHOTONICS AND  
PLASMONICS

<sup>1</sup>Groupe d'Optique de Champ Proche - LRC CEA n°DSM-08-36, Laboratoire Interdisciplinaire Carnot de Bourgogne. UMR CNRS 6303- Université de Bourgogne, France, <sup>2</sup>SiNaPS lab./SP2M, UMR-E CEA/UJF-Grenoble1, INAC, Grenoble, F38054, France, <sup>3</sup>CNRS/UJF-Grenoble1/CEA LTM, 17 rue des Martyrs, 38054 Grenoble cedex9, France.

Received  
19 March 2013Accepted  
10 July 2013Published  
26 July 2013

Correspondence and  
requests for materials  
should be addressed to  
B.C. (benoit.cluzel@u-  
bourgogne.fr)

Particles manipulation with optical forces is known as optical tweezing. While tweezing in free space with laser beams was established in the 1980s, integrating the optical tweezers on a chip is a challenging task. Recent experiments with plasmonic nanoantennas, microring resonators, and photonic crystal nanocavities have demonstrated optical trapping. However, the optical field of a tweezer made of a single microscopic resonator cannot be shaped. So far, this prevents from optically driven micromanipulations. Here we propose an alternative approach where the shape of the optical trap can be tuned by the wavelength in coupled nanobeam cavities. Using these shapeable tweezers, we present micromanipulation of polystyrene microspheres trapped on a silicon chip. These results show that coupled nanobeam cavities are versatile building blocks for optical near-field engineering. They open the way to much complex integrated tweezers using networks of coupled nanobeam cavities for particles or bio-objects manipulation at a larger scale.

The desired property for an optical tweezer is generally a sharp localisation of light which maximises the optical gradient forces compared to the radiation pressure<sup>1–3</sup>. In free space, it is achieved inside the beam waist of a laser focused by a high numerical aperture microscope objective<sup>4</sup>. In integrated optics, among the library of photonics structures, the dielectric nanocavities<sup>5–9</sup> and the plasmonic nanoantennas<sup>10,11</sup> with a strong field localisation are efficient optical traps for single particles, molecules or biological elements. However, these resonant structures provide an optical field distribution set by their design. Thus the resulting optical trap cannot be tuned dynamically. Here, we propose to use coupled cavities which light localisations are addressable by the wavelength<sup>5,12,13</sup> to overcome this limitation. In this work, we fabricated different coupled nanobeam cavities on a silicon optofluidic chip and we have explored their properties for tweezing polystyrene particles and micromanipulating them dynamically<sup>14</sup>. By properly tuning the trapping wavelength with respect to the near-field properties of different coupled cavities<sup>15</sup>, we first report proof-of-concept demonstrations of particles counting and microscopic motion sensing. Then we demonstrate that coupled cavities are efficient building blocks for the future development of tuneable integrated tweezers devoted to the micromanipulation of the particles.

## Results

The silicon nanobeam cavities considered here are photonic crystal Fabry Perot cavities integrated on silicon on insulator waveguide<sup>16,17</sup>. These one dimensional cavities can be coupled together through their evanescent field on the edge of the silicon waveguide as well as through a central photonic crystal mirror. To provide a robust coupling between the cavities<sup>18</sup> but also to minimise the perturbation of the cavity field by the particles to manipulate<sup>8</sup>, the cavities exhibit moderate quality factor ( $Q \sim 3,000$ ) for a  $0.6 (\lambda/n)^3$  volume, where  $\lambda$  is the resonance wavelength and  $n$  the cavity refractive index. The silicon photonic chip is then combined to a static microfluidic cell filled by 1  $\mu\text{L}$  volume of green fluorescent polystyrene (PS) 1  $\mu\text{m}$  microspheres solution. As depicted in Fig. 1, the optofluidic cell is mounted onto a fluorescence microscope allowing the observation of the individual particle motion while the cavities are loaded at their resonance wavelength(s). For the experiments shown hereafter, the input power required for optical trapping was only few microwatts which is comparable to the most recent report in this field<sup>19</sup>. Such a low value is of a prime importance since temperature and flow gradients due to loaded cavities must be minimised on the chip to envisage future optofluidics applications. Here, the local temperature enhancement inside the Fabry Perot cavities was estimated from the resonance wavelength redshift of the loaded cavity compared to the cold cavity at room temperature. For the input powers considered throughout this work, the redshift was measured to almost 50 pm which corresponds to a local heating lower than 1K inside the Fabry Perot cavity according to the thermo-optics coefficient of silicon<sup>20–22</sup> as well as compared to our earlier works<sup>23</sup>.

Two nanobeam cavities coupled laterally through a 200 nm air slot are studied first. This coupling scheme allows to enhance the local field inside the slot and thus to sense any refractive index change in their proximity<sup>12,24</sup>.

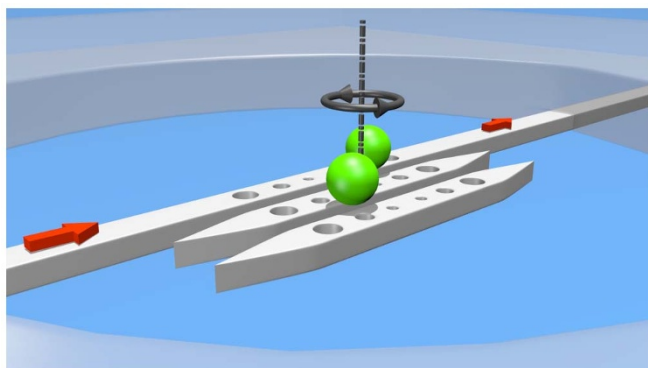


**Figure 1 | Coupled nanobeam cavities integrated inside a microfluidic cell.** A dimer made of two polystyrene microspheres is trapped by the coupled cavities and its orientation is controlled by the wavelength.

A scanning electron micrograph (SEM) view of the two cavities is shown on Fig. 2 and the 3D electromagnetic calculations of the electric field in water at resonance above the cavities are overlaid. The local field enhancement results from the constructive interference between the modes of each individual cavity<sup>12</sup>. The nearly perfect matching between the cavities is preliminary checked by Scanning Near-field Optical Microscopy (SNOM) observations available in the Supplementary Section 1 and then the optical trapping experiments are conducted. The nanobeam is loaded at the resonance wavelength while the particles motion above the cavities and the nanobeam transmittance are monitored simultaneously. The nanobeam transmittance is plotted in Fig. 2b and the pictures of the particles motion extracted from Supplementary Movie S1 are shown in Fig. 2c. The experiment shows the successive trapping of two particles. Due to the near-field interactions between the dielectric particles and the field confined inside the slotted structure (the 3D electromagnetic calculations of these interactions are available in the Supplementary Section 1), the resonance wavelength is redshifted by the presence of the particles inside the optical trap<sup>25</sup>. For this reason, each particle trapping event is associated with a 10% damping of the nanobeam transmittance. This sensitivity to the trapping events is comparable to that one reported for other integrated photonic devices used for optical trapping<sup>5,26</sup>. However, the sharp field localisation inside the slot<sup>12</sup> enables here an enhanced sensitivity to the microscopic motion of the trapped particles. A closer view of the transmittance signal shows small amplitude fluctuations. The latter are directly correlated to the submicrometric motion of the particles

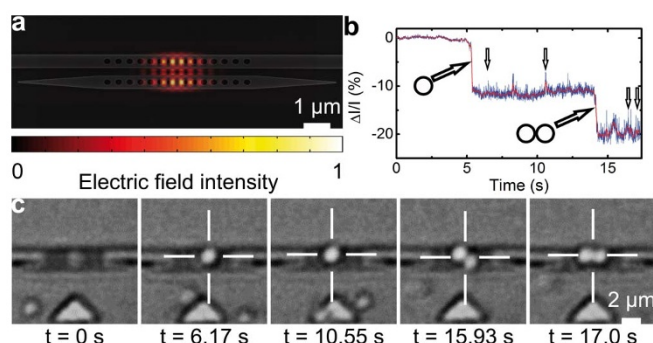


**Figure 2 | Trapping and sensing the particles with coupled cavities.** a, Scanning electron micrograph view of the coupled cavities overlaid with the 3D Finite Difference Time Domain calculation of the resonant mode in water. b, Nanobeam transmittance recorded during the trapping experiment. c, Selected snapshots at different instants of the experiment pointed on b, by the arrows extracted from supplementary Movie S1.

inside the trap, as verified by observing Supplementary Movie S1. As a result, the sensitivity shown here enables stored particles counting but also permits to sense their submicrometric motions of the particle inside the trap. As we demonstrated hereafter, we have next considered other coupling schemes between the cavities for controlling these microscopic motions by means of shapeable optical traps.

Our approach for the trap shaping relies on the coupling engineering between the cavities<sup>13</sup> to give rise to an addressable redistribution of the resonant mode. For instance, the two cavities can be coupled to each other through the central photonic crystal mirror. If they are perfectly identical, the coupled structure supports two identical resonant modes delocalised in both cavities. Introducing a nanometrical variation between the length of the two cavities breaks this symmetry<sup>18</sup>. Depending on the resonant wavelength, a preferential redistribution of the mode inside one or the other cavity occurs. Hence changing the operating wavelength enables to switch the predominant optical trap from one cavity to the other. For a 2 nm difference between the cavity lengths, the 3D FDTD calculations of the two resonant modes in water are overlaid to the SEM view of the fabricated structure in Fig. 3. The transmittance spectrum showing the two resonances is displayed in Fig. 3b and the experimental observation of the corresponding modes by SNOM is provided in Supplementary Section 2.

As shown in Supplementary Movie S2, a single particle as well as two particles trapped together move from a cavity to the other as the resonance wavelength is tuned. The particles move here without being released since they slide inside the same trap which is balanced by the wavelength from one cavity to the other. Figure 3c and 3d show the pictures selected from Supplementary Movie S2 emphasising this experimental observation. The particle average speed inside the trap is measured to  $4 \mu\text{m}\cdot\text{s}^{-1}$  for a single particle and it is reduced to  $3 \mu\text{m}\cdot\text{s}^{-1}$  for two particles due to an increased drag. The linear translation of the trapped particles observed here is triggered by the wavelength changes and may open promising perspectives for the microscopic positioning of particles on predetermined trapping sites.

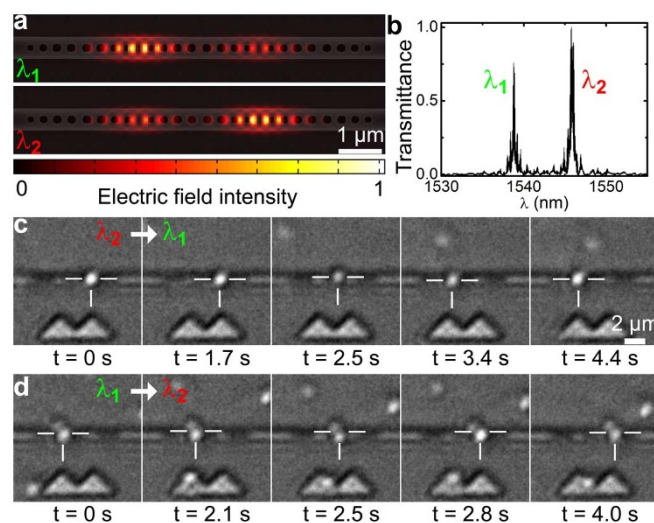


**Figure 3 | Micro positioning of trapped particles with detuned coupled cavities.** a, Scanning electron micrograph view of the coupled cavities overlaid with the 3D Finite Difference Time Domain calculation of the resonant modes in water. b, Transmittance spectrum of the detuned coupled cavities in water. The two resonance wavelengths are referred as  $\lambda_1$  and  $\lambda_2$ . c, Selected snapshots at different times of the experiment extracted from supplementary Movie S2 showing the single particle motion from a cavity to the other actuated by a wavelength change from  $\lambda_2$  to  $\lambda_1$ . d, same as c, but with two trapped particles and actuated by a wavelength change from  $\lambda_1$  to  $\lambda_2$ .

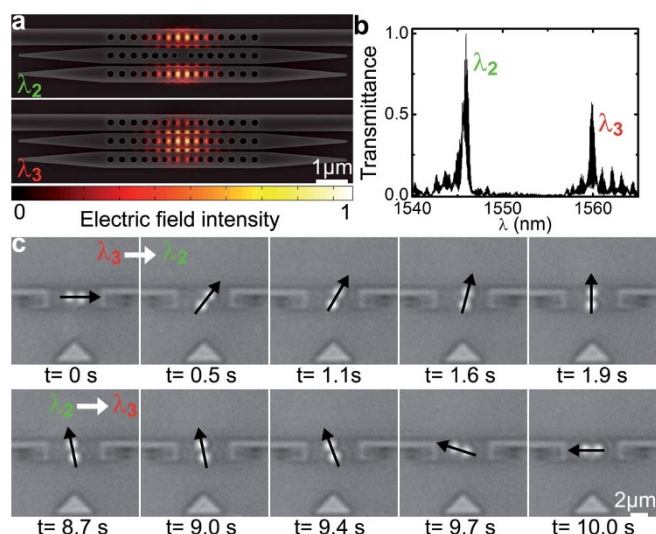


**Figure 4 | Orientation control of a dimer with three coupled cavities.** a, Scanning electron micrograph view of the coupled cavities overlaid with the 3D Finite Difference Time Domain calculation of considered resonant modes  $\lambda_2$  and  $\lambda_3$  in water. c, Transmittance spectrum of the coupled cavities showing the resonant modes  $\lambda_2$  and  $\lambda_3$  in water. d, Selected snapshots at different instants of the experiment extracted from supplementary Movie S3 showing the rotary motion of the dimer triggered by the resonant modes  $\lambda_2$  and  $\lambda_3$ .

We also believe that an accurate control of the absolute position of the particle between the cavities could be achieved by using a dual wavelengths excitation with balanced intensities.

Another approach for micromanipulation is to use the multiple interferences processes involved between multiple coupled cavities. In this case, the cavities can be switched on and off independently in respect to the symmetry axis of the coupled structure<sup>13</sup>. For instance, for three cavities coupled through air gaps as shown in Fig. 4, three resonant wavelengths switch on respectively the central cavity only ( $\lambda_3$ ), the two external ones ( $\lambda_2$ ) and all together ( $\lambda_1$ ).

The SNOM observations of these three modes are provided in Supplementary Section 3. The two modes in water at  $\lambda_2$  and  $\lambda_3$  displayed on the SEM view of the fabricated structure in Fig. 4a also provide an additional degree of freedom to control the orientation of an anisotropic assembly of trapped particles. To illustrate this, we manipulated a dimer made of two trapped particles. As shown on the pictures of Fig. 4c, a dimer trapped at  $\lambda_3$  is confined and orientated along the central cavity. The dimer orientation is then changed by tuning the wavelength of the laser to  $\lambda_2$ . As shown on Supplementary Movie S3, a counter clockwise  $90^\circ$  rotation of the dimer is observed. Then tuning the laser to  $\lambda_3$  enforces a new rotation of the dimer. Remarkably, the rotation is once again observed counter clockwise which gives rise to a global rotary motion. In more detail, from the experimental observations, we determined the angular speed ( $\omega$ ) between two orthogonal orientations. From  $\lambda_3$  to  $\lambda_2$ ,  $\omega_{2-3}$  equals to  $0.84 \text{ rad}\cdot\text{s}^{-1}$  while from  $\lambda_2$  to  $\lambda_3$ ,  $\omega_{3-2} = 1.39 \text{ rad}\cdot\text{s}^{-1}$ . These differences correspond to the different optical torques associated to the two optical traps. However, the main limitation for the rotary motion remains the switching time between the operating wavelengths. For proof-of-concepts demonstrations, the switch was made manually which results in the sequential motion observed in Supplementary Movie S3 but this could be greatly enhanced by means of an optical switch. A proper control of the switch according to the particle angular speed could permit to achieve a continuous rotary motion. An accurate control of the absolute orientation of the dimer could also be achieved by using a dual wavelengths excitation with balanced intensities. Applying this micromanipulation technique to other

types of anisotropic particles, for instance to nanowires or metallic dimers, could permit a dynamical control of their orientation for applications in surface enhanced Raman spectroscopy (SERS) as well as any other optical technique which is polarization sensitive.

## Discussion

In summary, by properly engineering the near-field coupling between photonic crystal cavities on a silicon optofluidic chip, we manage to configure a predetermined set of optical forces distributions addressable individually by the wavelength. Different functionalities such as trapping, counting, moving and rotating particles are built by taking benefit from the versatility of the coupling geometry between the cavities. Compared to the existing tweezers integrated on a silicon chip<sup>27,28</sup>, the near-field coupling between the cavities provides here an additional degree of freedom to address by the wavelength optical traps with different shapes. This capability opens innovative ways for all optical control of microparticle and bio-object micromanipulation in nanoscale science without a free space optical tweezing system.

Despite the small number of coupled cavities considered in this work, the near-field coupling give rise to significantly different optofluidic functions relying on optical gradient forces. A step forward will consist in increasing the number of coupled cavities into a complex photonic array merging the different coupling schemes and thus enabling the manipulation of trapped particles at a larger scale. In this case, new optical strategies with multiple operating wavelengths will be required to achieve a simultaneous and parallel control of the trapped particles.

At last, the reported proof-of-concepts experiments were carried out with purely dielectric particles. However, the near-field interactions with micro and nano sized objects not only depends on the electromagnetic field distribution but also on their intrinsic properties such as their size, their geometry, or their dielectric and magnetic constants. Different behaviours are thus expected for these different objects inside the optical traps. Once the prerequisite analysis on individual species will be conducted, the manipulation of heterogeneous trapped particles could be envisaged in a near future. As shown for dielectric spheres<sup>29</sup>, this could permit for instance the development of an all integrated light templating technique for building heterogeneous materials.

## Methods

The photonics structures are fabricated using the standard microelectronics techniques. We used a 100 keV electron beam to lithography the structure and then we etched the processed 200 mm SOI wafer with a chloride induced coupled plasma machine. The optical characterisations of the samples were made on typical optical end-fire coupling bench experiments. The microfluidics cells used on the photonics samples are made with a spincoated polydimethylsiloxane layer patterned with a rectangular aperture allowing a  $1 \mu\text{L}$  volume of colloidal solution in the cell. This PDMS layer is deposited and bonded on the photonic sample with oxygen plasma. The cell is firstly filled with colloidal solution and sealed by a microscope thin cover slip glass. The photonics structures are visualised with a vision column and a microscope objective arranged around a homemade bright field and fluorescence vision set-up. The nanocavities are lightened through a lensed fiber with a Tunics tunable laser TE polarized source with a 150 nm wide near-infrared spectral range. For the trapping experiment we add in an erbium doped fiber amplifier with output power of 200 mW in the C and L telecommunication bands. The optical signal is collected with a microscope objective and detected with an InGaAs photodiode. The effective power injected inside the waveguide is measured to few microwatts at the output. The detector is linked to a high bandwidth oscilloscope through a current amplifier. A user interface synchronises the camera image recording (over the photonics structures) with the optical signal monitoring.

1. Ashkin, A. Optical Levitation by Radiation Pressure. *Appl. Phys. Lett.* **19**, 283 (1971).
2. Ashkin, A. Acceleration and trapping of particles by radiation pressure. *Phys. Rev. Lett.* **24**, 156–159 (1970).
3. Ashkin, A., Dziedzic, J. M. & Yamane, T. Optical trapping and manipulation of single cells using infrared laser beams. *Nature* **330**, 769–771 (1987).
4. Grier, D. G. A revolution in optical manipulation. *Nature* **424**, 810–6 (2003).





5. Lin, S. & Crozier, K. B. Planar silicon microrings as wavelength-multiplexed optical traps for storing and sensing particles. *Lab chip* **11**, 4047–51 (2011).
6. Mandal, S., Serey, X. & Erickson, D. Nanomanipulation using silicon photonic crystal resonators. *Nano lett.* **10**, 99–104 (2010).
7. Cai, H. & Poon, A. W. Optical manipulation and transport of microparticles on silicon nitride microring-resonator-based add-drop devices. *Opt. letters* **35**, 2855–7 (2010).
8. Renaut, C. *et al.* Assembly of microparticles by optical trapping with a photonic crystal nanocavity. *Appl. Phys. Lett.* **100**, 101103 (2012).
9. Chen, Y.-F., Serey, X., Sarkar, R., Chen, P. & Erickson, D. Controlled photonic manipulation of proteins and other nanomaterials. *Nano lett.* **12**, 1633–7 (2012).
10. Juan, M. L., Righini, M. & Quidant, R. Plasmon nano-optical tweezers. *Nature Photonics* **5**, 349–356 (2011).
11. Wong, H. M. K. *et al.* On-a-chip surface plasmon tweezers. *Appl. Phys. Lett.* **99**, 061107 (2011).
12. Foubert, K. *et al.* An air slotted nanoresonator relying on coupled high Q small V Fabry Perot nanocavities. *Appl. Phys. Lett.* **94**, 251111 (2009).
13. Cluzel, B. *et al.* Addressable subwavelength grids of confined light in a multislot nanoresonator. *Appl. Phys. Lett.* **98**, 081101 (2011).
14. Dholakia, K. & Čižmár, T. Shaping the future of manipulation. *Nature Photon.* **5**, 335–342 (2011).
15. Lalouat, L. *et al.* Subwavelength imaging of light confinement in high Q/small V photonic crystal nanocavity. *Appl. Phys. Lett.* **92**, 111111 (2008).
16. Foresi, J. S., Villeneuve, P. R., Ferrera, J. *et al.* Photonic-band-gap microcavities in optical waveguides. *Nature* **390**, 143–145 (1997).
17. Velha, P. *et al.* Ultracompact silicon-on-insulator ridge-waveguide mirrors with high reflectance. *Appl. Phys. Lett.* **89**, 171121 (2006).
18. Foubert, K. *et al.* Influence of dimensional fluctuations on the optical coupling between nanobeam twin cavities. *Phys. Rev. B* **85**, 235454 (2012).
19. Descharmes, N., Dharanipathy, U. P., Diao, Z., Tonin, M. & Houdré, R. Observation of Backaction and Self-Induced Trapping in a Planar Hollow Photonic Crystal Cavity. *Phys. Rev. Lett.* **110**, 123601 (2013).
20. Nazarova, N. A., Romanova, G. I. & Yas'Kov, A. D. Refractometric characteristics of silicon. *Sov. J. Opt. Technol* **55**, 220–224 (1988).
21. Cocorullo, G., Della Corte, F. G. & Rendina, I. Temperature dependence of the thermo-optic coefficient in crystalline silicon between room temperature and 550 K at the wavelength of 1523 nm. *Appl. Phys. Lett.* **74**, 3338 (1999).
22. Jellison, G. E. & Burke, H. H. The temperature dependence of the refractive index of silicon at elevated temperatures at several laser wavelengths. *J. Appl. Phys.* **60**, 841 (1986).
23. Velha, P. *et al.* Ultra-High Q/V Fabry-Perot microcavity on SOI substrate. *Opt. Express* **15**, 16090–6 (2007).
24. Deotare, P. B., McCutcheon, M. W., Frank, I. W., Khan, M. & Lončar, M. Coupled photonic crystal nanobeam cavities. *Appl. Phys. Lett.* **95**, 031102 (2009).
25. Lalouat, L. *et al.* Near field interactions between a subwavelength tip and a small volume photonic crystal nanocavity. *Phys. Rev. B* **76**, 041102 (2007).
26. Lin, S., Zhu, W., Jin, Y. & Crozier, K. B. Surface-enhanced Raman scattering with Ag nanoparticles optically trapped by a photonic crystal cavity. *Nano lett.* **13**, 559–63 (2013).
27. Hellesø, O. G., Løvhaugen, P., Subramanian, A. Z., Wilkinson, J. S. & Ahluwalia, B. S. Surface transport and stable trapping of particles and cells by an optical waveguide loop. *Lab chip* **12**, 3436–40 (2012).
28. Lin, S. & Crozier, K. B. An integrated microparticle sorting system based on near-field optical forces and a structural perturbation. *Opt. Express* **20**, 3367–74 (2012).
29. Jaquay, E., Martínez, L. J., Mejia, C. A. & Povinelli, M. L. Light-assisted, templated self-assembly using a photonic-crystal slab. *Nano lett.* **13**, 2290–4 (2013).

## Acknowledgements

C.R., B.C. and F.F. acknowledge the regional council of Burgundy for financial funding in the framework of the PHOTCOM project. This project has been performed in cooperation with the Labex ACTION program (contract ANR-11-LABX-01-01).

## Author contributions

C.R. and D.P. fabricated the samples. B.C. and E.P. conceived the experiment. C.R., J.D. and E.P. developed the experimental set up. C.R. performed the experiments. C.R., B.C. and L.L. analysed all the experimental data. L.L. performed all the computer simulations. B.C. wrote the manuscript. E.H. and F.F. guided the work.

## Additional information

**Supplementary information** accompanies this paper at <http://www.nature.com/scientificreports>

**Competing financial interests:** The authors declare no competing financial interests.

**How to cite this article:** Renaut, C. *et al.* On chip shapeable optical tweezers. *Sci. Rep.* **3**, 2290; DOI:10.1038/srep02290 (2013).



This work is licensed under a Creative Commons Attribution-NonCommercial-ShareAlike 3.0 Unported license. To view a copy of this license, visit <http://creativecommons.org/licenses/by-nc-sa/3.0>